Draft version November 1, 2004
Preprint typeset using LaTeX style emulateapj v. 4/9/03

MULTICOLOR SURFACE PHOTOMETRY OF LENTICULARS I. THE DATA

Sudhanshu Barway[1], Y. D. Mayya[2], Ajit K. Kembhavi[3], and S. K. Pandey[1]

Draft version November 1, 2004

ABSTRACT

We present in this paper multicolor surface and aperture photometry in the B, V, R and K' bands for a sample of 34 lenticular galaxies from the UGC catalogue. From surface photometric analysis, we obtain radial profiles of surface brightness, colors, ellipticity, position angle and the Fourier coefficients which describe the departure of isophotal shapes from purely elliptical form and find the presence of dust lanes, patches and ring like structure in several galaxies in the sample. We obtain total integrated magnitudes and colors and find that these are in good agreement with the values from the RC3 catalogue. Isophotal colors are correlated with each other, following the sequence expected for early-type galaxies. The color gradients in lenticulars are more negative than the corresponding gradients in ellipticals. There is a good correlation between $B-V$ and $B-R$ color gradients, and the mean gradient in the $B-V, B-R$ and $V-K'$ colors are -0.13 ± 0.06, -0.18 ± 0.06, -0.25 ± 0.11 magnitude per dex in radius respectively.

Subject headings: galaxies: lenticular - galaxies: photometry - galaxies: fundamental parameters

1. introduction

Hubble (1936) introduc4794(h)-335.78.82hTd[(0.74252(e)-1.22283(n)25.687758.7598Td4(h)S420.841(l9.96264T742528.285.8911

Table 1. Basic parameters of the sample galaxies

Galaxy		Type (T)	Diameter (arcmin)	z	m_{ph}	M_B
UGC 00080	NGC 0016	−3.0	1.8x1.0	0.010194	12.50	−20.93
UGC 00491	NGC 0252	−1.0	1.5x1.1	0.016645	13.40	−21.65
UGC 00859	NGC 0473	0.0	1.7x1.1	0.007118	13.20	−19.82
UGC 00926	NGC 0499	−2.5	1.6x1.3	0.014673	13.00	−21.55
UGC 01250	NGC 0670	−2.0	2.0x1.0	0.012352	13.10	−20.76
UGC 01823	NGC 0890	−3.0	2.5x1.7	0.013323	12.50	−22.31
UGC 01964	NGC 0940	−2.0	1.2x1.0	0.017319	13.40	−21.64
UGC 02039	NGC 0969	−2.0	1.7x1.6	0.015054	13.50	−21.51
UGC 02187	NGC 1040	−2.0	1.7x0.8	0.016054	14.00	−21.06
UGC 02322	NGC 1106	−1.0	1.8x1.8	0.014467	13.70	−21.39
UGC 03087		−2.0	0.8x0.6	0.033010	14.20	−22.28
UGC 03178	NGC 1671	−2.0	1.1x0.9	0.021270	13.90	−21.63
UGC 03452	NGC 2208	−2.0	1.7x1.0	0.018763	14.00	−21.26
UGC 03536		−2.0	1.1x0.6	0.015641	14.40	−20.86
UGC 03567		−2.0	1.0x0.8	0.020164	14.20	−21.26
UGC 03642		−2.0	1.5x1.1	0.015004	13.50	−21.47
UGC 03683		−2.0	2.0x1.3	0.019076	14.10	−21.53
UGC 03699	NGC 2332	−2.0	1.5x1.0	0.019467	14.00	−21.52
UGC 03792		0.0	1.8x1.3	0.020608	14.00	−21.46
UGC 03824		−2.0	0.9x0.8	0.017866	14.40	−20.76
UGC 04347	NGC 2563	−2.0	2.1x1.5	0.014944	13.70	−21.06
UGC 04767		−2.0	1.3x1.1	0.024127	14.00	−21.80
UGC 04901	NGC 2804	−2.0	2.2x2.0	0.028099	14.00	−22.23
UGC 05292	NGC 3032	−2.0	2.0x1.8	0.005114	13.00	−19.43
UGC 06013		−2.0	0.9x0.8	0.021898	13.90	−21.69
UGC 06389	NGC 3648	−2.0	1.3x0.8	0.006631	13.50	−19.50
UGC 06899	NGC 3971	−2.0	1.4x1.2	0.022489	13.90	−21.75
UGC 07142	NGC 4143	−2.0	2.3x1.4	0.003616	12.00	−20.03
UGC 07473	NGC 4350	−2.0	3.0x1.4	0.004140	11.50	−20.48
UGC 07880	NGC 4638	−3.0	2.2x1.4	0.003883	12.20	−19.64
UGC 07933	NGC 4673	−5.0	1.0x0.9	0.022856	13.70	−21.99
UGC 08675	NGC 5273	−2.0	2.8x2.5	0.003616	12.70	−19.24
UGC 09200	NGC 5580	−2.0	1.8x1.8	0.010814	13.60	−20.46
UGC 09592	NGC 5784	−2.0	1.9x1.8	0.017912	13.70	−21.78
UGC 11178	NGC 6599	−2.0	1.3x1.2	0.010120	13.70	−20.30
UGC 11356	NGC 6703	−2.5	2.5x2.3	0.008209	12.40	−21.14
UGC 11781		−2.0	1.4x1.1	0.015501	13.70	−21.74
UGC 11972	NGC 7248	−2.5	1.7x0.9	0.014627	13.60	−21.22
UGC 12443	NGC 7539	−2.0	1.5x1.2	0.020174	13.70	−21.88
UGC 12655		−2.0	1.4x0.9	0.017269	14.00	−21.24

Note. — Columns (1) and (2) give the UGC catalogue number and NGC catalogue number respectively, column (3) gives the morphological type from the RC3 catalogue, columns (4) and (5) give the diameter (in arcmin) along the major and minor axis respectively, and the redshift from NASA Extragalactic Database (NED), column (6) give the photographic magnitude from the UGC catalogue and column (7) give the absolute B magnitude for $H_0 = 50\,\mathrm{km\,sec^{-1}\,Mpc^{-1}}$.

eral Catalogue of Galaxies (UGC). The UGC is essentially complete to a limiting major-axis diameter of one arcmin and/or to a limiting apparent magnitude of 14.5 on the blue prints of the Palomar Observatory Sky Survey (POSS) (Nilson 1973) limited to the sky north of declination −2.5°. For our sample we selected galaxies with apparent blue magnitude brighter than $m_B = 14$, diameter $D_{25} < 3$ arcmin and declination in the range $5 < \delta < 64°$. The sample galaxies are listed in Table 1. Our sample, though not complete, is representative of lenticular galaxies in the field with the above properties.

2.2. *Optical imaging*

Our optical BVR-band observations were carried out with the *Observatorio Astrofísico Guillermo Haro* 2.1-m telescope at Cananea, Mexico. We used a Tektronics CCD of 1024×1024 pixel format at the $f/12$ Cassegrain focus of the telescope with 3×3 pixel binning, resulting in a scale of $0\farcs6$ pixel^{-1} and a field of view of $3\farcm4 \times 3\farcm4$. Typically two exposures each of ten, five and five minutes in B, V, and R bands respectively were taken for each galaxy. Exposure times were reduced if the central pixels were close to saturation. Twilight sky exposures were taken for flat-fielding purposes. Several bias frames pixels wer

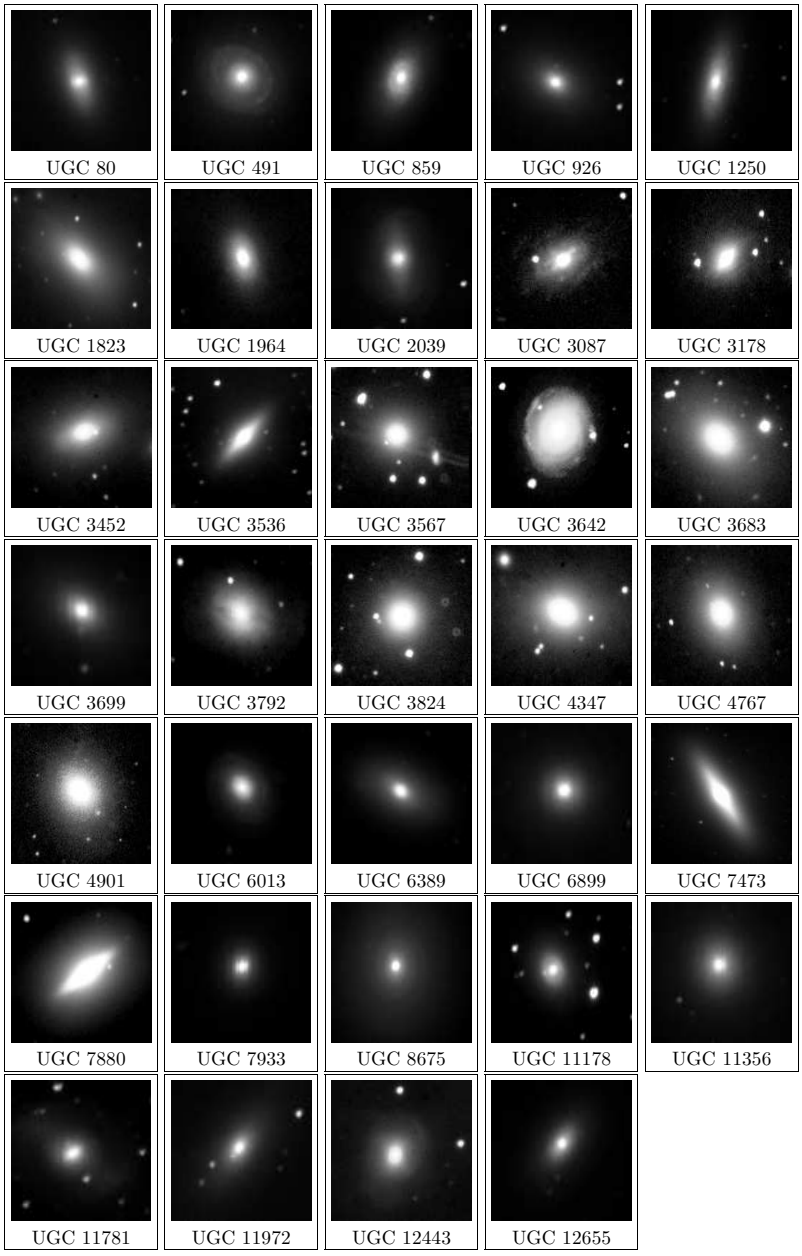

FIG. 1.— Gray-scale representation of color composite images of our sample galaxies (see § 2.4).

cal reducer configuration $f/4.5$ in all our observations. This results in a spatial resolution of $0\farcs85$ pixel^{-1} and a total field of view of $3\farcm6 \times 3\farcm6$. Each K' observation consisted of a sequence of object and sky exposures, with the integration time of an individual exposure limited by the sky counts (or in some cases the nucleus), which was kept well below the non-linear regime of the detector. A typical K' image sequence consisted of 10 exposures, six on the object and four on the sky. The net exposure times were typically of 10 minutes. A series of twilight and night-sky images were taken for flat-fielding purposes. The K' observations were carried out in four runs in December 2000, March 2001, October 2001 and March 2002.

The sky conditions for both optical and near infrared observations were generally photometric and the seeing *FWHM* was in the range $1\farcs5$–$2\farcs5$ on different nights. The average sky brightness was 21.14, 20.72, 20.18 and 12.27 magnitude arcsec^{-2} in the B, V, R and K' bands, respectively. The sky brightness in the K' band also includes the background emitted by the warm optics.

2.4. *Data reduction*

The basic data reduction for both the optical and near infrared K' images involved subtraction of the bias and sky frames, division by flat field frames, registration of the images to a common co-ordinate system and then stacking all the images of a given galaxy in each filter. Night to night variations of the optical bias frames were negligible, and hence bias frames of an entire run were stacked together using the median algorithm to form a master bias frame, which was then subtracted from all the other frames. Preparation of the optical flat fields followed the conventional technique, wherein bias subtracted flats were stacked and the resultant frame was normalized to its mean value to form a master flat in each filter. Bias subtracted images of the program galaxies were divided by the normalized flat field in the corresponding filter. The optical images suffered from a stray light problem that resulted in a gradient in the sky background, which roughly ran through one of the diagonals of the CCD chip. The gradient was found to be stable throughout each run and the mean counts scaled linearly with exposure time. After several experiments, we found that the best way to get rid of the gradient was to subtract a mean blank sky image from the data images. For this purpose, special blank fields were observed in each filter with exposure times matching the typical exposure times of the object frames. In the December 2001 run, three blank sky frames were used in each filter to prepare a median gradient image, while in the February 2002 run, six frames were used. The adopted procedure eliminated any gradient from the sky background.

For the K' images, a bias frame taken immediately before an object exposure was subtracted as part of the data acquisition. A master K' flat field for each night of observing was prepared as follows. The night-sky flats were first stacked and then subtracted from stacked twilight flats. The frames obtained in this fashion for each run were then combined and normalized to the mean value of the resultant frame to form a master K' flat. The sky frames of each sequence of observations were combined and the resultant image was subtracted from each of the object frames to get a sky-subtracted image. Flat fielding was done by dividing the sky subtracted images of the object by the normalized master flat. The resulting images were aligned to a common co-ordinate system using common stars in the frames and then combined using the median operation. Only good images (as defined in the CAMILA manual — see Cruz-Gonzalez et al. 1994) were used in the K' combination. The resulting combined K' images were aligned to corresponding images from the Digitized Sky Survey (DSS). As a final step of the reduction procedure, the mutually aligned optical images were aligned to the K' image coordinate system. The transformed star positions in the images agreed to within $0\farcs2$ as judged from the coordinates of common stars.

All image reductions were carried out using the Image Reduction and Analysis Facility (IRAF[4]) and the Space Telescope Science Data Analysis System (STSDAS). The IRAF external package *color* was used to make color composite images, by combining images taken in three different bands, B, V and R or V, R and K'. Gray-scale representation of these color composite images are shown in Fig. 1, where North is up and East is to the left.

2.5. *Photometric calibration*

Dipper Asterism stars in the M 67 field were observed to enable accurate photometric calibration of our optical observations. The stars in this field span a wide color range ($-0.05 < B-V < 1.35$), which includes the range of colors of the program galaxies, and hence are suitable for obtaining the transformation coefficients to the Cousins BVR system defined by Bessell (1990). The transformation equations are

$$B = b_0 + \alpha_B + \beta_B(b_0 - v_0), \quad (1)$$

$$V = v_0 + \alpha_V + \beta_V(b_0 - v_0), \quad (2)$$

$$R = r_0 + \alpha_R + \beta_R(v_0 - r_0), \quad (3)$$

where B, V and R are standard magnitudes, b_0, v_0 and r_0 are extinction corrected instrumental magnitudes, α_B, α_V and α_R are the zero points and β_B, β_V and β_R the color coefficients in bands B, V and R respectively. Typical extinction coefficients for the observatory (0.20, 0.11 and 0.07 for B, V and R bands respectively) were used. Considering that the objects and the standard stars were observed as close to the meridian as possible, and in none of the cases the airmass exceeded 1.3, the error introduced due to possible variation in the extinction coefficients is less than 0.02 magnitude. Coefficients α and β were obtained by using the BVR standard magnitudes of Chevalier & Ilovaisky (1991). Resulting values of α and β are given in Table 3. The relatively large color coefficient on the R-band calibration is due to the non-standard nature of the filter used in the observations. The stability of the α on a given night was checked using at least two other standard fields from the Landolt Selected Areas (Landolt 1992). The standard fields observed during our runs are SA 110−232, PG 2336+004, Rubin 149 and PG 1323−086. Overall, the zero points within a single night agreed to within 0.02 magnitudes.

[4] IRAF is distributed by National Optical Astronomy Observatories, which are operated by the Association of Universities for Research in Astronomy, Inc., under cooperative agreement with the National Science Foundation.

Table 2. Log of observations

Galaxy	Date of Observation		Exposure Time (sec)				Seeing *FWHM* (arcsec)			
	BVR	K'	*B*	*V*	*R*	K'	*B*	*V*	*R*	K'
UGC 00080	04-10-2002	10-10-2001	1200	360	540	750	2.24	2.07	2.03	1.56
UGC 00491	05-10-2002	12-10-2001	1200	600	600	750	1.85	2.18	2.18	1.52
UGC 00859	14-12-2001	09-10-2001	1200	600	600	900	2.41	2.81	2.64	1.76
UGC 00926	05-10-2002	10-10-2001	1200	360	540	750	1.80	1.66	1.78	1.49
UGC 01250	04-10-2002	10-10-2001	1200	600	600	900	2.31	2.10	2.01	1.48
UGC 01823	14-12-2001	09-10-2001	1200	600	600	750	2.43	2.78	2.67	1.61
UGC 01964	14-12-2001	09-10-2001	1200	600	600	900	2.10	2.09	2.18	1.60
UGC 02039	05-10-2002	12-10-2001	1200	600	600	600	1.91	2.11	2.01	1.64
UGC 02187	...	10-10-2001	....	...	...	900	...	...	...	1.47
UGC 02322	...	09-10-2001	....	...	...	780	...	...	...	1.49
UGC 03087	08-02-2002	24-03-2002	1200	540	540	480	2.16	1.98	2.14	2.06
UGC 03178	09-02-2002	23-03-2002	1200	600	600	320	2.02	1.87	1.87	1.75
UGC 03452	14-12-2001	16-12-2000	1200	600	600	600	2.55	2.76	2.63	1.58
UGC 03536	08-02-2002	26-03-2002	1200	540	540	105	2.14	2.01	2.05	1.54
UGC 03567	07-02-2002	28-02-2002	1200	600	600	750	2.17	1.97	2.04	1.92
UGC 03642	09-02-2002	26-02-2002	1200	720	720	750	1.86	2.04	1.90	1.48
UGC 03683	08-02-2002	23-03-2002	1200	600	600	750	2.26	2.26	1.97	2.07
UGC 03699	05-10-2002	12-10-2001	600	360	540	750	2.58	2.58	2.59	1.89
UGC 03792	14-12-2001	10-10-2001	1200	600	600	750	2.28	2.69	2.43	1.85
UGC 03824	07-02-2002	26-03-2002	1800	600	600	105	2.13	2.13	2.24	1.66
UGC 04347	14-12-2001	08-03-2001	1200	600	600	540	2.51	2.71	2.55	1.88
UGC 04767	08-02-2002	24-03-2002	1200	600	600	600	2.42	2.07	2.08	1.92
UGC 04901	09-02-2002	26-03-2002	....	600	600	105	...	1.75	1.85	1.45
UGC 05292	...	07-06-2001	....	...	...	900	...	...	...	1.67
UGC 06013	07-02-2002	08-02-2001	....	600	600	840	...	2.50	2.07	1.64
UGC 06389	08-02-2002	23-03-2002	1200	540	540	700	1.92	2.05	2.03	1.89
UGC 06899	08-02-2002	23-03-2002	1200	600	600	840	1.96	1.97	1.94	1.27
UGC 07142	...	23-03-2002	....	...	...	450	...	...	...	2.07
UGC 07473	09-02-2002	22-03-2002	900	450	270	260	2.12	2.13	2.08	1.43
UGC 07880	09-02-2002	25-03-2002	1200	270	600	500	2.37	2.64	2.41	1.79
UGC 07933	07-02-2002	08-03-2002	....	540	540	840	...	2.47	2.26	1.79
UGC 08675	08-02-2002	22-03-2002	1200	600	540	310	2.04	1.91	1.82	1.63
UGC 09200	...	07-03-2001	....	...	...	840	...	...	...	1.50
UGC 09592	...	24-03-2002	....	...	....	600	...	...	...	1.92
UGC 11178	04-10-2002	22-03-2002	900	600	600	240	2.15	2.06	2.20	1.39
UGC 11356	05-10-2002	23-03-2002	1200	240	360	420	1.91	1.91	1.91	1.80
UGC 11781	04-10-2002	09-10-2001	900	600	600	540	1.99	1.94	2.07	1.83
UGC 11972	05-10-2002	10-10-2001	900	540	360	900	2.07	1.79	1.78	1.50
UGC 12443	14-12-2001	12-10-2001	1200	600	600	900	2.87	2.89	2.92	1.56
UGC 12655	04-10-2002	09-10-2001	1200	600	600	120	2.24	1.98	2.12	1.59

Night-to-night variation of the zero point was also within 0.02 magnitudes.

The detector and filter system combination that we used for the near infrared observations is identical to that used in the observations of standards by Hunt et al. (1998), and hence the color coefficients are expected to be negligibly small. We verified this by observing fields AS17 and AS36, which contain stars spanning a wide range of colors. We observed at least 2 standard fields each night, each field containing more than one star and some fields such as AS17 containing 5 stars. The K'-band zeropoints was obtained for each night as the mean of zero points from different stars and the average value is $\alpha_{K'} = 20.15 \pm 0.05$.

For reddening corrections due to galactic extinction we adopt the values given by Schlegal et al. (1998) for each filter in the optical range. For near infrared observations we use the extinction law given by Rieke et al. (1985). When galaxies at different redshift are seen through a fixed passband, the collected light comes from different wavelength ranges in the rest frame of the respective galaxies. K-correction is used to transform the rest frame magnitudes of each object to the passband of the filter. We have used an approximate form of the K-correction, applicable for small z, from Persson et al. (1979), Frei et al. (1994) and Fukugita et al. (1995). For the four filters we have, $K_B = 4.4z$, $K_V = 3.24z$, $K_R = 2.12z$ and $K_{K'} = -3z$ respectively, where z is the redshift of the galaxy. We have listed the combination of Galactic extinction and K-correction for individual galaxies in Table 4.

3. analysis

3.1. *Sky background*

An accurate estimation of the sky background is a crucial step in surface photometric analysis, as even small uncertainties in determining the sky can lead to significant errors in the estimation of the galaxy surface brightness and color profiles, especially where the surface brightness becomes comparable to or less than the sky brightness. In those cases where the galaxy image is small enough that the frame contains portions of the sky unaffected by the galaxy, it is possible to estimate the sky using the "boxes method" (see Peletier et al. 1990a), where the background is estimated from a series of boxes chosen avoiding the sample galaxy, foreground stars and any other contaminating objects which may be present. We have used 20 boxes of size 5×5 pixels near the corners of the CCD frame, and have adopted the mean of

Table 3. Zero points and transformation coefficients for optical observations

Filter	Zero point α	Color coefficient β
February 2002		
B	22.88±0.03	−0.095±0.016
V	23.49±0.02	0.075±0.010
R	22.45±0.05	−0.408±0.081
October 2002		
B	22.60±0.03	−0.095±0.016
V	23.21±0.04	0.075±0.010
R	22.15±0.03	−0.408±0.081

the median count in these boxes as the sky background. The rms dispersion over the mean of 20 boxes is found to be 0.6% of the mean in the B, V, and R bands and 0.2% of the mean in the K' band. When a galaxy is so large that the whole frame is affected by it, use of the boxes method leads to overestimation of the background. In such cases, the background can be determined by fitting a power-law of the form I(r) = sky + I(0) $r^{-\alpha}$ to the outer parts of the surface brightness profile. Following Jorgensen et al. (1992) and Goudfrooij et al. (1994), we fit the function to the region of the profile with $r > 50''$ typically, separately for $\alpha = 2$ and 3, and use the mean of the respective best-fit constant values as the background. The error in the sky background estimation is taken to be half the difference of the sky values obtained for the two fits. We have used both the techniques for all galaxies in our sample, and find that in most cases the two methods agree within ~ 0.005 magnitude (i.e. 1σ difference), because of the small size of the galaxies relative to the CCD frame. In the case of the galaxies UGC 4347, 7473, 7880, 8675 and UGC 11356, which cover most of the frame, the power-law fit provides a background which is ~ 0.06 magnitude (i.e. 10σ difference) fainter than the boxes method, and we adopt the former as the background estimation. In the K' band images, the background is already subtracted from the many individual frames for each galaxy during the preprocessing stage (see §2.4). However, to check for any residual background which may be present in processed frames used in the analysis, we have again applied the two techniques for the background estimation. We find that the two estimates agree very well (~ 0.0006 magnitude, except in two cases where the agreement is within ~ 0.001 magnitude).

3.2. *Surface Photometry : Isophotal analysis*

We have fitted ellipses to the isophotes in our B, V, R and K' band images, using the task ELLIPSE in the STSDAS package available in IRAF. The fitting algorithm used is described in detail by Jedrzejewski (1987), and uses the intensity distribution along a trial ellipse, which can be expressed as a Fourier series

$$I(\phi) = I_0 + \sum_n a_n \sin(n\phi) + \sum_n b_n \cos(n\phi), \qquad (4)$$

where ϕ is the ellipse eccentric anomaly, I_0 is the mean intensity along the ellipse and a_n, b_n are harmonic amplitudes.

The fitting was started a few arcseconds from the center of the galaxy image to minimize the effect of seeing, and stopped at the isophotes where the mean count becomes comparable to three times the error in the sky background. Stars, bad pixels etc. were identified in the first round of the fitting procedure and masked in the next run. All the parameters including the center of the ellipse were allowed to vary during the fitting. Variation in ellipse center was found to be small ($\sim$ 1.2 arcsec), which provides a check on the accuracy of the sky subtraction. We repeated the fitting process with different modes of sampling and different starting major-axis lengths to check the stability of the extracted parameters.

The fitting procedure provides the mean intensity (surface brightness), the ellipticity and the position angle of the major-axis of the best fit ellipse, as a function of the semi-major axis length. The B band surface brightness profile, and the $B-V, B-R$ and $V-K'$ color profiles are shown for all the galaxies in Fig. 2. The profiles of the ellipticity, position angle and the Fourier coefficients a_3, a_4, b_3, b_4 respectively in the B, R and K' bands for one galaxy (UGC 7880) are shown in Fig. 3. Tables and plots of surface brightness and color profiles as well as the profiles of the ellipticity, position angle and the Fourier coefficients a_3, a_4, b_3, b_4 respectively in the B, R and K' bands for all the galaxies in the sample are available at *http://iucaa.ernet.in/∼sudhan/s0.html*. Some description of the profiles for individual galaxies is provided in the Appendix.

Color measurements of galaxies involving frames with different seeing full width at half maximum ($FWHM$) can lead to errors at small radii, and in particular within the seeing disk which has to be approached for measuring nuclear colors. These errors have been discussed by Franx et al. (1989), Peletier et al. (1990a) and Goudfrooij et al. (1994), who have derived a cutoff radius for color profiles and discarded colors measured inside this limit, which is usually $2 \times FWHM$. Idiart et al. (2002) used a method of equalization of the $FWHMs$ to reduce error due to different seeing $FWHM$ but this method is feasible only if the frames involved in color measurement are observed in quick succession. For our observations the seeing $FWHM$ was nearly the same for the optical B, V and R bands, but significantly better in K' band as

Table 4. Integrated magnitudes and colors

Galaxy	B	$B-V$	$B-R$	$V-K'$	Galactic extinction + K correction			
					B	$B-V$	$B-R$	$V-K'$
UGC 00080	13.01±0.04	0.95±0.01	1.54±0.01	3.34±0.04	0.25	0.06	0.10	0.20
UGC 00491	13.46±0.05	0.97±0.02	1.61±0.01	3.36±0.05	0.32	0.07	0.13	0.27
UGC 00859	13.41±0.03	0.78±0.01	1.28±0.01	3.22±0.06	0.41	0.09	0.16	0.30
UGC 00926	13.32±0.05	1.02±0.01	1.66±0.01	3.59±0.03	0.36	0.08	0.14	0.29
UGC 01250	13.53±0.03	0.81±0.01	1.37±0.01	3.32±0.04	0.36	0.08	0.14	0.29
UGC 01823	12.58±0.03	0.96±0.01	1.53±0.01	3.37±0.04	0.39	0.09	0.15	0.31
UGC 02039	13.38±0.08	0.97±0.02	1.59±0.02	3.48±0.05	0.57	0.13	0.22	0.44
UGC 03087	14.60±0.07	0.62±0.05	1.09±0.05	3.72±0.18	0.42	0.10	0.17	0.35
UGC 03452	13.70±0.07	1.09±0.01	1.69±0.01	3.69±0.04	0.74	0.17	0.29	0.56
UGC 03536	13.39±0.09	1.02±0.01	1.60±0.01	3.62±0.03	0.54	0.12	0.21	0.42
UGC 03567	14.36±0.06	1.03±0.01	1.61±0.01	3.54±0.05	0.44	0.10	0.18	0.36
UGC 03642	13.51±0.05	0.91±0.02	1.50±0.02	3.39±0.07	0.26	0.06	0.11	0.23
UGC 03683	13.72±0.06	1.04±0.01	1.64±0.01	3.76±0.04	0.48	0.11	0.19	0.39
UGC 03699	14.13±0.12	1.08±0.01	1.71±0.01	3.64±0.02	0.45	0.10	0.18	0.37
UGC 03792	14.07±0.05	1.10±0.01	1.75±0.01	3.57±0.05	0.38	0.09	0.15	0.32
UGC 03824	14.22±0.05	0.99±0.01	1.57±0.01	3.30±0.05	0.31	0.07	0.13	0.27
UGC 04347	13.40±0.04	1.01±0.01	1.57±0.01	3.57±0.04	0.25	0.06	0.10	0.22
UGC 04767	14.26±0.05	0.99±0.01	1.53±0.01	3.55±0.05	0.19	0.04	0.08	0.21
UGC 06389	13.57±0.03	0.93±0.01	1.45±0.01	3.35±0.05	0.11	0.02	0.04	0.10
UGC 06899	14.01±0.04	0.88±0.01	1.42±0.01	3.37±0.06	0.17	0.04	0.08	0.19
UGC 07473	12.01±0.02	0.93±0.01	1.46±0.01	3.39±0.03	0.13	0.03	0.05	0.10
UGC 07880	12.14±0.03	0.91±0.01	1.39±0.01	3.24±0.04	0.12	0.03	0.05	0.09
UGC 08675	12.50±0.03	0.80±0.02	1.31±0.02	3.20±0.09	0.05	0.01	0.02	0.05
UGC 11178	13.71±0.06	0.89±0.01	1.27±0.01	3.68±0.04	0.70	0.16	0.27	0.51
UGC 11356	12.29±0.07	0.95±0.01	1.53±0.01	3.52±0.04	0.41	0.09	0.16	0.31
UGC 11781	14.23±0.07	1.18±0.01	1.87±0.01	3.86±0.03	1.12	0.26	0.43	0.82
UGC 11972	13.90±0.06	1.14±0.01	1.82±0.01	3.79±0.02	0.76	0.17	0.29	0.56
UGC 12443	13.94±0.04	0.99±0.01	1.52±0.01	3.36±0.05	0.52	0.12	0.21	0.42
UGC 12655	14.09±0.05	0.93±0.01	1.53±0.01	3.50±0.04	0.32	0.07	0.13	0.27

Note. — Column (2) gives the measured uncorrected total B magnitude, column (3) to (5) give the measured $B-V$, $B-R$, and $V-K'$ color indices, columns (6) to (9) give the combination of Galactic foreground extinction and K correction.

indicated by Table 2. We have therefore degraded the K' images to the mean *FWHM* of the optical band images for each galaxy. The $V-K'$ color profiles shown in Fig. 2 were obtained using the degraded K' band images.

3.3. *Integrated magnitudes*

In this work we obtain the total magnitude of each galaxy in all the bands by integrating the light within the isophote corresponding to $\mu_{\rm B} = 25$ mag arcsec^{-2} in each band. To obtain the $B-V, B-R$ and $V-K'$ colors, however, we integrate out only to the radius at which the error in $\mu_{\rm B}$ is 0.1 mag arcsec^{-2} (the radius where the dotted horizontal line intersects the $\mu_{\rm B}$ profile in Fig. 2). The colors obtained in this manner are consistent with those obtained using total magnitude as defined above, within the estimated errors. However, the errors on integrated colors obtained in this manner are substantially lower (typically 0.01 vs 0.04 in $B-V$, 0.01 vs 0.04 in $B-R$, and 0.05 vs 0.12 in $V-K'$ colors). We also obtain total K' magnitudes measured to $\mu_{\rm K'} = 20$ mag arcsec^{-2} in order to make comparison with 2MASS photometry. The measured total B magnitudes and $B-V, B-R$ and $V-K'$ colors along with the estimated errors for the 29 galaxies in the sample for which we have the necessary data are shown in Table 4. In Fig. 4 (left panel) we have compared our photometry with that in the literature. We have plotted (from bottom to top) the difference between (i-ii) our B magnitude and $B-V$ color and those of RC3, (iii) our B magnitude and that of UGC and (iv) our K' magnitude measured inside the isophote $\mu_{\rm K'}$ = 20 mag arcsec^{-2} and that of 2MASS, all against our B magnitude. Agreement between our B magnitude with that of RC3 is within the expected errors for all except two galaxies. Our total $B-V$ colors are systematically around 0.04 magnitude bluer than those of RC3. On the other hand, if we compare the $B-V$ color obtained by integrating only upto $\mu_{\rm B} = 21$ mag arcsec^{-2} (*bulge color*), the agreement between our

Table 5. Color gradients

Galaxy	r1 (arcsec)	r2 (arcsec)	$\Delta(B-V)/\Delta\log r$	$\Delta(B-R)/\Delta\log r$	$\Delta(V-K')/\Delta\log r$
UGC 00080	3.40	28.05	−0.09±0.01	−0.14±0.04	−0.22±0.02
UGC 00491	3.40	51.00	−0.25±0.03	−0.26±0.03	−0.25±0.00
UGC 00859	....	.....	.....	.....	.....
UGC 00926	3.40	34.00	−0.21±0.01	−0.24±0.01	−0.23±0.02
UGC 01250	....	....	.....	.....	−0.78±0.02
UGC 01823	3.40	34.00	−0.01±0.00	−0.02±0.01	−0.20±0.01
UGC 02039	3.40	09.35	−0.16±0.01	−0.23±0.01	−0.29±0.00
UGC 03087	....	....	.....	.....	.....
UGC 03452	3.40	09.35	−0.12±0.00	−0.15±0.00	−0.40±0.00
UGC 03536	3.40	09.35	−0.14±0.00	−0.19±0.00	−0.21±0.00
UGC 03567	3.40	09.35	−0.09±0.00	−0.11±0.00	−0.22±0.00
UGC 03642	3.40	13.60	−0.25±0.00	−0.30±0.00	−0.20±0.02
UGC 03683	3.40	13.60	−0.16±0.00	−0.16±0.00	−0.35±0.05
UGC 03699	3.40	17.00	−0.05±0.01	−0.12±0.01	−0.33±0.01
UGC 03792	3.40	17.00	−0.34±0.01	−0.54±0.01	−0.72±0.02
UGC 03824	3.40	21.25	−0.18±0.01	−0.19±0.01	−0.06±0.04
UGC 04347	3.40	22.95	−0.06±0.00	−0.09±0.00	−0.29±0.01
UGC 04767	3.40	18.70	−0.12±0.01	−0.21±0.01	0.12±0.02
UGC 06389	3.40	22.95	−0.15±0.00	−0.23±0.01	−0.27±0.01
UGC 06899	3.40	17.85	−0.19±0.01	−0.20±0.01	−0.23±0.01
UGC 07473	3.40	17.00	−0.14±0.00	−0.21±0.00	−0.42±0.01
UGC 07880	3.40	16.15	−0.18±0.01	−0.23±0.01	−0.26±0.01
UGC 08675	5.95	53.55	−0.09±0.00	−0.11±0.01	−0.19±0.01
UGC 11178	3.40	17.85	−0.10±0.01	−0.17±0.01	−0.29±0.02
UGC 11356	3.40	21.25	−0.13±0.01	−0.19±0.01	−0.24±0.01
UGC 11781	3.40	08.50	−0.12±0.00	−0.15±0.00	−0.45±0.02
UGC 11972	3.40	19.55	−0.08±0.01	−0.11±0.01	−0.25±0.01
UGC 12443	3.40	14.45	−0.10±0.00	−0.18±0.01	−0.16±0.01
UGC 12655	3.40	14.45	−0.17±0.00	−0.24±0.01	−0.29±0.01

Table 6. Comparison of color gradients

	$\Delta(B-V)/\Delta\log r$	$\Delta(B-R)/\Delta\log r$	$\Delta(V-K')/\Delta\log r$
Our sample	-0.13 ± 0.06 (25)	-0.18 ± 0.06 (25)	-0.25 ± 0.11 (25)
Ellipticals (Peletier et al. 1990a & b)	-0.04 ± 0.01 (12)	-0.09 ± 0.02 (30)	-0.16 ± 0.19 (12)
Bulges of disk galaxies (Peletier & Balcells 1997)	...	-0.19 ± 0.16 (30)	...

Note. — The number of galaxies used to obtain the listed mean values are indicated in brackets. See § 4 for details.

object. We exclude these two galaxies from further analysis.

3.4. *Dust*

We have used optical and K' band data to study the spatial distribution of dust. We have obtained extinction map in magnitude $A_\lambda = -2.5\log(I_{\lambda,\ \rm obs}/I_{\lambda,\ \rm model})$, where $I_{\lambda,\ \rm obs}$ is the observed image in same band, and $I_{\lambda,\ \rm model}$ is the smooth version of this image, obtained using the best fit ellipse parameters. Extinction map particularly helping in identifying non-axisymmetric structure. Color maps too are of help in identifying features with wavelength dependent intensity. We have noticed from the color and extinction maps that the lenticular galaxies UGC 3178, UGC 3536, UGC 3792, UGC 4347, UGC 7473 and UGC 7880 show clear evidence of the presence of dust in the form of lanes or patches. In all these cases there are differences in the ellipticity and position angle profiles, as well as in the higher order Fourier coefficients profiles, in the different bands. This indicates that such differences could be used as indicators of the possible presence of dust, even when the dust is not otherwise discernible (see e. g. Peletier et al. 1990a, Goudfrooij et al. 1994). The lenticular galaxy UGC 3792 has a very prominent dust lane along the major axis (see the appendix for details). We will present elsewhere a detailed study of the dust in our sample of galaxies.

4. color gradients

It is the usual practice to parameterize the color gradient over the galaxy as the slope $\Delta(B-V)/\Delta\log r$, which is evaluated by making a straight line fit between an inner and an outer radius to the color profiles. The inner cutoff limit (r1) is taken to be ∼1.5 times the seeing FWHM (Peletier et al. 1990a), so that seeing effects are lessened. The outer limit (r2) is taken to be the point along the major axis at which the error on the mean surface brightness of the fitted ellipse reaches 0.1 mag arcsec^{-2}. It is seen from Fig. 2 that plots of color against the logarithm of the semi-major axis for most of our sample galaxies, have a reasonably linear form between the inner and outer cutoff. There are some cases (UGC 859, 1250

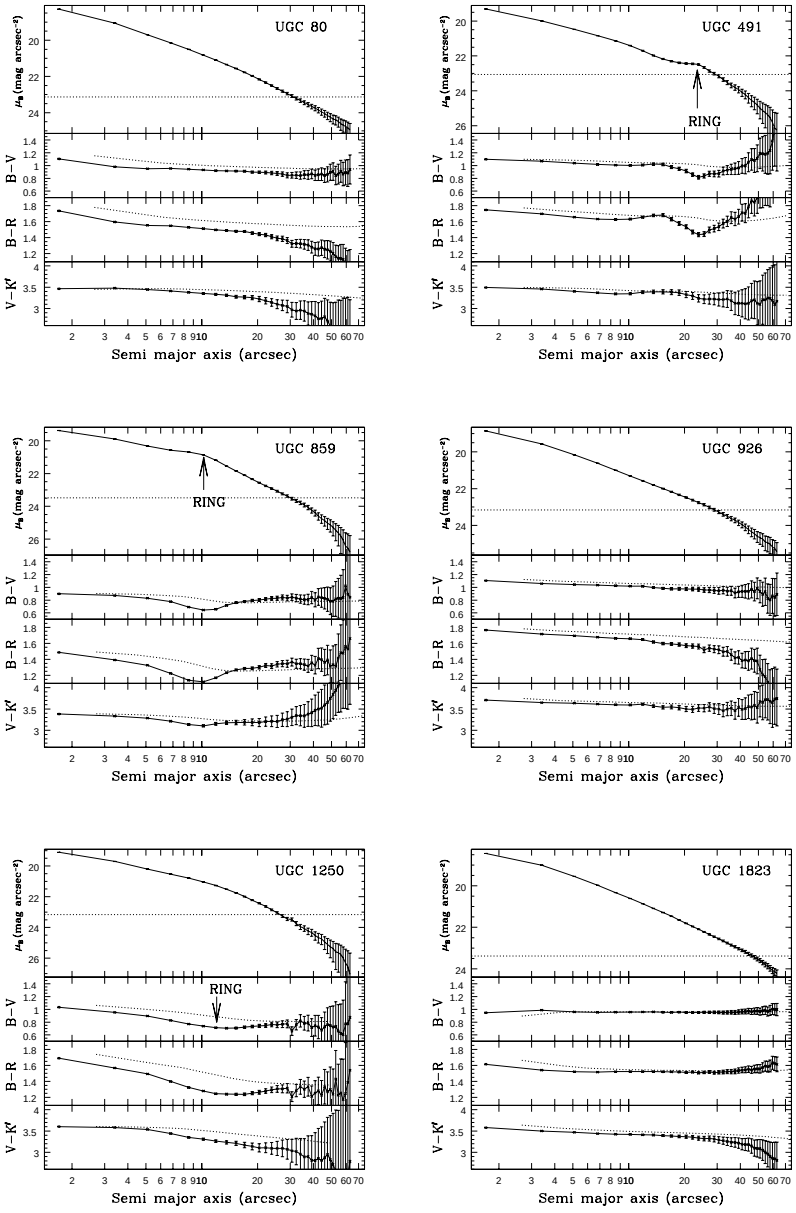

FIG. 2.— Surface brightness and color profiles along the major axis of sample galaxies.For each galaxy, B-band surface brightness and the $B-V$, $B-R$ and $V-K'$ color profiles (solid lines) are given in separate panels. The integrated color of the galaxy in successive elliptical apertures is shown by the dotted curve. The galaxy B-band intensity corresponding to 10% of the sky brightness (or equivalently an error of 0.1 mag arcsec^{-2}) is indicated by the dotted line in the top panel. The error bars on the surface brightness profiles correspond to 1% error in the estimation of the sky background. Error bars on the color profiles are estimated by quadratically adding the uncorrelated part of the errors on the two magnitudes that contribute to the color.

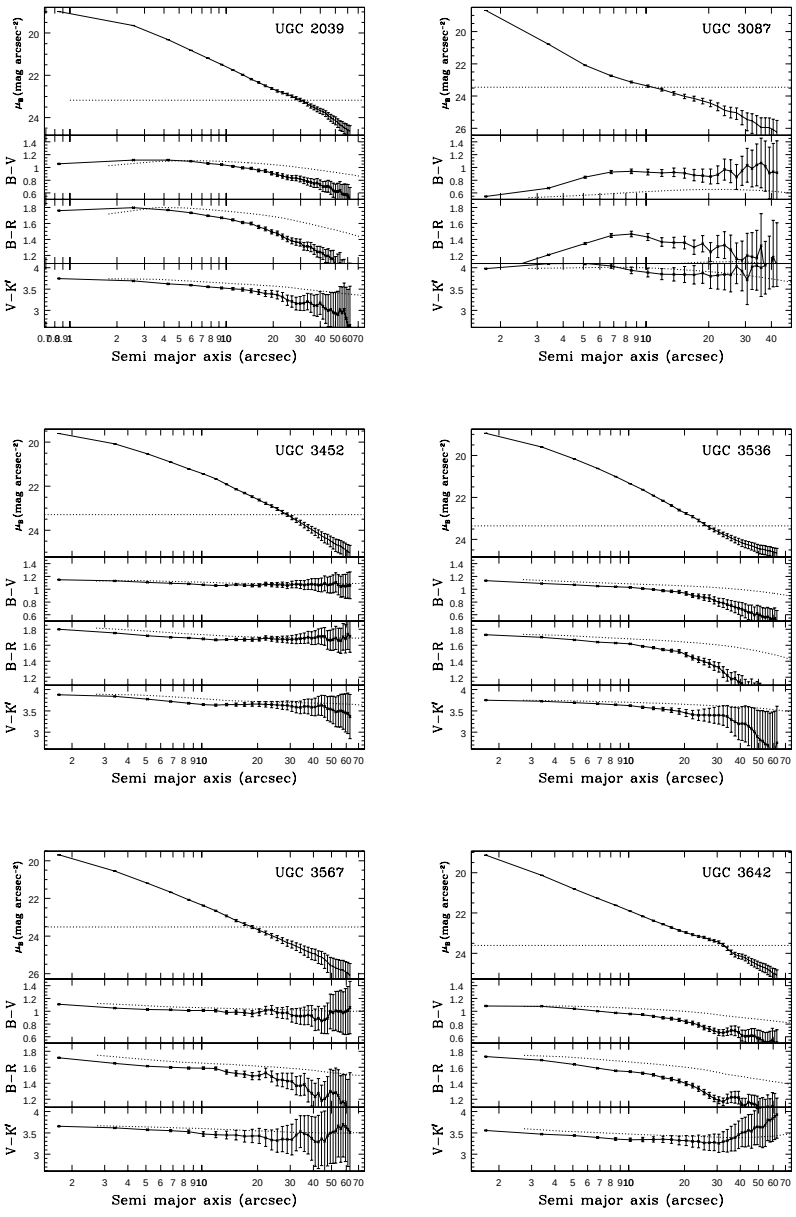

FIG. 2 (continued)

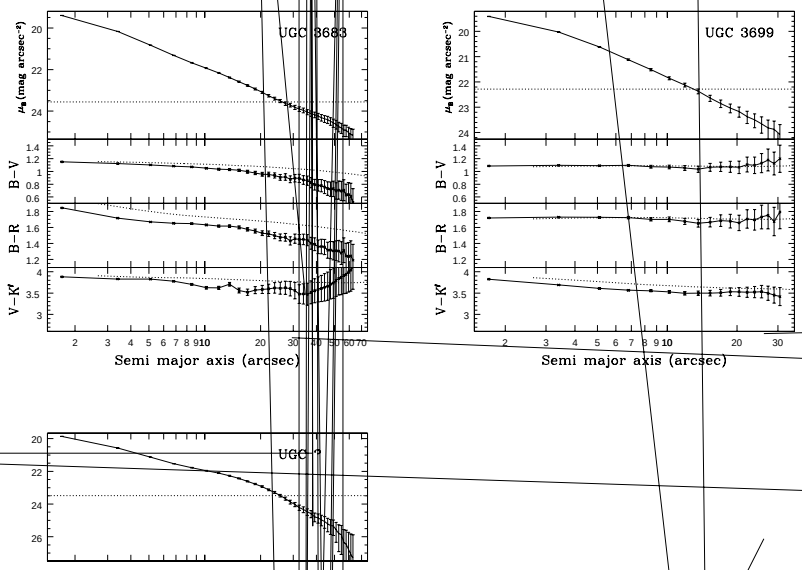
UGC 3683
UGC 3699
μ_B (mag arcsec^{-2})
B−V
B−R
V−K'
Semi major axis (arcsec)
Semi major axis (arcsec)

UGC ?

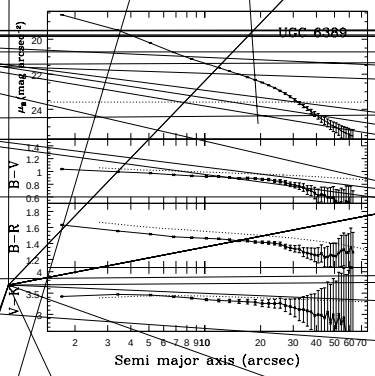
UGC 6389
μ_B(mag arcsec^{-2})
B−V
B−R
V−R
Semi major axis (arcsec)

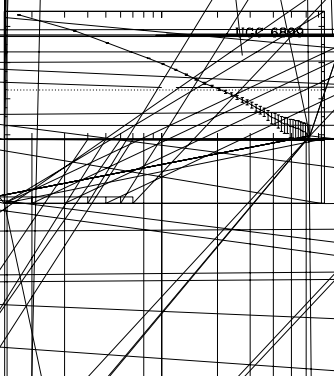
UGC 6809
μ_B(mag arcsec^{-2})

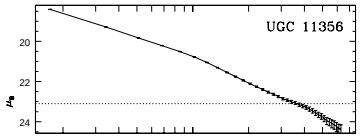
UGC 11356
20
22
24
μ_B

and 3087) for which the color profiles are non-linear between r1 and r2 because of the presence of a strong ring (UGC 859, 1250) or an AGN (UGC 3087), which makes reliable estimation of the color gradient is difficult. The $B-V, B-R$ and $V-K'$ color gradients for our galaxies are given in Table 5.

The colors of the galaxies in our sample become bluer outwards, in keeping with the trend observed in ellipticals. The only exception to this is the positive gradient in the $V-K'$ color of the galaxy UGC 4767. After excluding the galaxy UGC 3792 (which has a prominent dust lane), the mean logarithmic gradients in the $B-V, B-R$ and $V-K'$ colors are -0.13 ± 0.06, -0.18 ± 0.06, -0.25 ± 0.11 magnitude per dex in radius respectively. A comparison of our mean color gradients with corresponding values from the literature for ellipticals and bulges of early-type spirals is shown in Table 6. The color gradients for lenticulars are more negative than the gradients for ellipticals, while the $B-R$ gradient for lenticulars is less negative than the corresponding gradient for bulges of early-type spirals. Our steeper color gradients could imply that the metallicity gradients are stronger in lenticulars and/or that there is more recent star formation in the outer parts of lenticulars as compared to those of ellipticals. Bothun & Gregg (1990) reported significant differences in the colors of bulges and disks in lenticulars which they interpret as being due to age difference, and not metallicity difference, between the bulge and disk components. The large rms error in the mean color gradient of our sample could be due to the different colors of the bulge and disk components and varying proportion of these in different lenticulars.

Correlation between different color gradients have been noted by various authors (Peletier et al. 1990a & b and Idiart et al. 2002) and have been used to derive information about the physical processes in galaxies. Such correlations are displayed in Fig. 5 for our sample. A clear correlation is seen between $B-V$ and $B-R$ gradients, with correlation coefficient 0.90 at a significance level better than 99.99 percent. Correlation between $B-V$ and $B-R$ gradient has been noticed for a sample of ellipticals by Peletier et al. (1990 a & b). From their data we obtain a correlation coefficient of 0.97 at a significance level better than 99.99 percent. The plot of $V-K'$ against $B-V$ gradients shows large scatter, and we do not see any correlation of the type reported by Peletier et al. (1990b), but it should be noted that they used only 13 galaxies to derive the correlation. It is necessary to investigate how the separate bulge and disk color gradients affect the total color gradients and hence the correlation between them. We will address in the future these issues using a bulge-disk decomposition technique which will allow us to study the color distribution in these components separately.

5. CONCLUSIONS

In this paper we have presented detailed multicolor surface photometry performed with a CCD in the B, V, R bands and a NICMOS detector in the K' band, for a sample of 34 lenticular galaxies from the UGC catalogue. The galaxies were chosen in an unbiased fashion from a subset of UGC lenticulars as explained in Section 2. We have obtained total integrated magnitudes and colors for all the galaxies using elliptical annuli from surface photometry, and find that these are in good agreement with values from the RC3 catalogue. Using isophotal analysis we have obtained radial profiles of the surface brightness, ellipticity, position angle, and higher order Fourier coefficients in all the bands. The profiles in the different bands are consistent with each other, and any differences can be attributed to the presence of dust and other features which produce wavelength dependent effects. We have used the surface brightness profiles to obtain color profiles, and logarithmic color gradients, and find that the gradients are negative, indicating that the colors of lenticulars become redder towards the center, as is the case with elliptical galaxies. We have shown that there is good correlation between $B-V$ and $B-R$ color gradients for lenticulars. Numerical profiles of all parameters that we have obtained from the isophotal analysis along with the color images are available at *http://www.iucaa.ernet.in/∼sudhan/s0.html*.

Our intention in obtaining the multiband data on lenticulars has been to study in detail these galaxies as a class, and to compare their properties with those of ellipticals and early type spirals. An important aspect of this study will be the decomposition of the lenticulars into bulge and disk components and the comparison of these separately with the bulges and disks in other types of galaxies where these components occur with varying degrees of prominence. We will use the results of the decomposition in a multiband study of the fundamental and photometric planes for lenticulars. We will also make a detailed study of the distribution of dust in lenticulars, particularly in those galaxies from our sample where there are prominent dust features and where we have multiband data at optical as well as near-infrared wavelengths.

The staff at OAGH and SPM are greatfully acknowledged for their help during the observations. SB and SKP thank IUCAA for hospitality and the use of facilities without which this work could not have been done and for providing funds for observations. AKK and SB thank INAOE for hospitality provided during there visits. We also thank the anonymous referee for several useful comments, which helped to improve the original manuscript. This research has made use of the NASA/IPAC Extragalactic Database (NED), which is operated by the Jet Propulsion Laboratory, California Institute of Technology, under contract with the National Aeronautics and Space Administration.

APPENDIX

In this appendix, we discuss structural properties of each galaxy, whenever isophotes in one or more bands depart from a smooth ellipse. The discussions are focused on any disagreement in the morphological classification in UGC and RC3 catalogs, presence of dust lane, change of ellipse-fit parameters (b4, PA or ellipticity), existence of any ring,

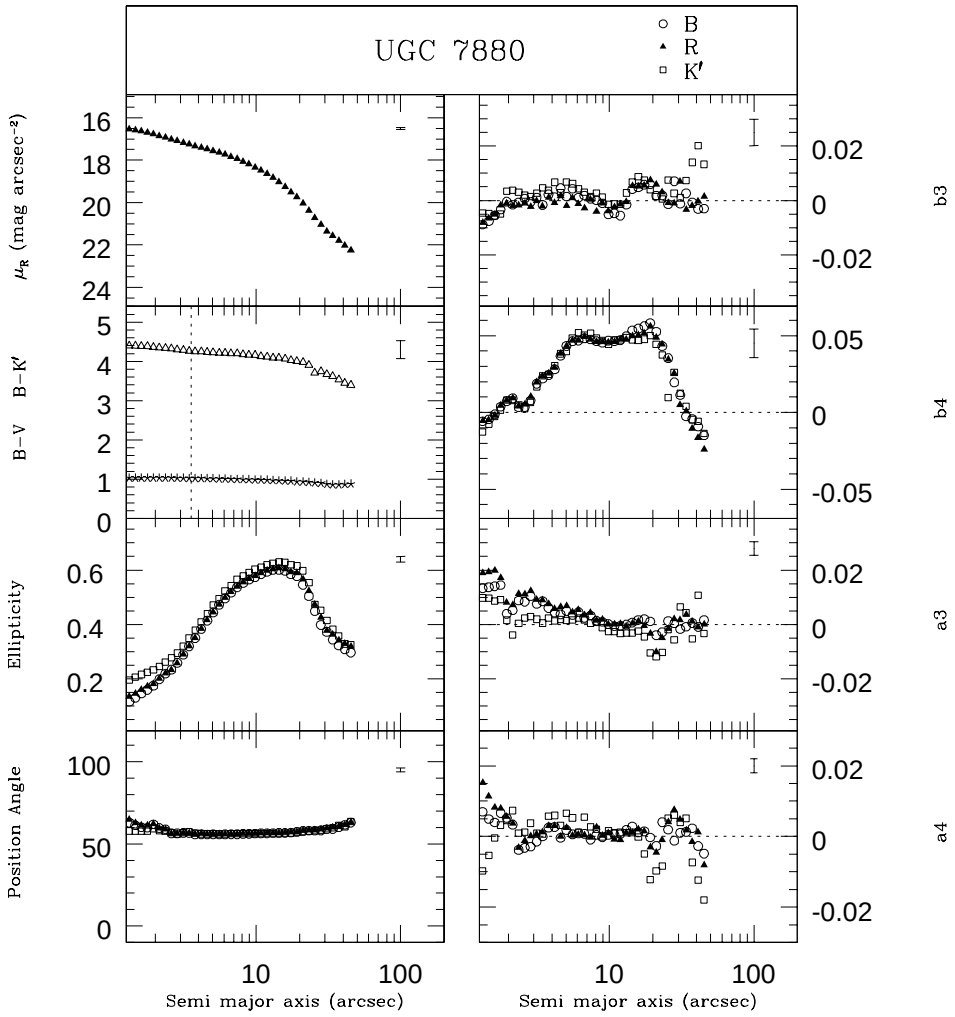

FIG. 3.— Isophotal profiles for the galaxy UGC 7880. See the text for details.

and any evidence of nuclear activity. Published information on any of these issues, if available, is noted. In total 12 galaxies (UGC 926, 1823, 3452, 3567, 3683, 3699, 3824, 6013, 6389, 6899, 11972 and 12443) are smooth lenticular galaxies without any identifiable feature in the direct images, the surface brightness profiles, color or extinction maps. Comments for the remaining galaxies follow.

UGC 80 : UGC 80 is a barred lenticular galaxy, having a very faint interacting companion. The faint bar is almost perpendicular to the galaxy major axis, and is clearly evident in the isophotal profile. The b_4 profile is indicative of a disky shape over the entire major-axis range explored. The ellipticity and position angle profiles show abrupt change at $r \simeq 5$ arcsec, where there is also a kink in the brightness profile. The $B-R$ color map of the galaxy shows a red feature near the center.

UGC 491 : UGC 491 is the brightest galaxy in a small group with NGC 0258 and NGC 0260. This galaxy is classified as S0 in the UGC catalogue and SA(r) in the RC3 catalogue. In the optical images it indeed shows a ring, which is also evident in the $B-R$ and $B-K'$ color maps. Ellipticity and position angle profiles show a change at $r \sim 21.5$ arcsec, which may be due to the presence of the ring.

UGC 859 : UGC 859 shows an internal ring, but it is classified as S0 in the UGC catalogue. The $B-R$ and $B-K'$ color maps of the galaxy show the ring as an inhomogeneous structure. A low surface brightness disk with some luminous spiral structure exists outside the ring. UGC 859 has been detected by IRAS and has flux densities of 1160 ± 33 mJy at 60 μm and 870 ± 319 mJy at 100 μm (Knapp et al. 1989). The b_4 coefficient is disky towards the outer region.

UGC 1250 : While this galaxy is classified as S0, the $B-R$ color map of the galaxy show a very clear, but distorted

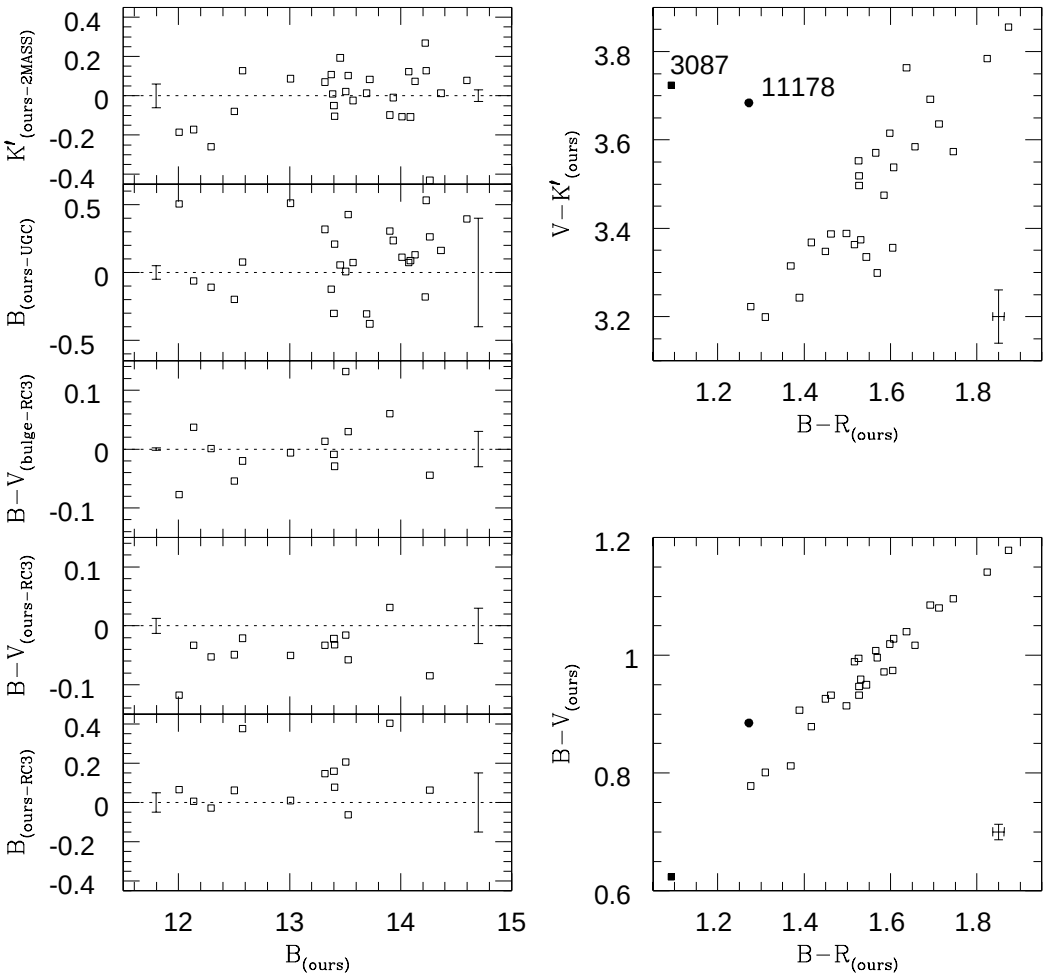

FIG. 4.— Comparison of our photometry with those in the literature. Left panel (from bottom to top): Difference between our B and that of RC3, our $B-V$ and that of RC3, our *bulge* $B-V$ and that of RC3, our B and that of UGC and our K' and that of 2MASS, plotted against our B magnitude. Error bars on our data (left), and the literature data (right) are plotted on the difference=0 line. Right panel: Color vs color plots from our data. Typical error bars are indicated on the bottom right part of the figure.

ring, just around the bulge. H$\alpha + [NII]$ observations by Pogge & Eskridge (1993) show copious HII regions across the disk. The b_4 profile is disky at all major-axis lengths, with the coefficient being larger in the inner region of the galaxy.

UGC 2039 : UGC 2039 is paired with UGC 2049. There is a rise in the ellipticity from 0.1 to 0.5 towards the outer region. The b_4 coefficient is disky in the outer region, which suggests the presence of a significant disk. The galaxy has been detected by IRAS at 60 and 100 μm. **UGC 3087 :** Previous studies of UGC 3087 have mainly concentrated on its nuclear activity. It is a strong radio source (3C120) and the optical spectrum suggests a Seyfert 1 nucleus (Tadhunter et al. 1993). It has a faint optical jet in the same apparent direction as the radio jet. The optical jet is clearly visible in our images and distorts isophotal profiles in the inner region.

UGC 3178 : A dust feature is clearly visible in the B band extinction map of this galaxy, and is also detectable from the isophotal analysis of B and K' band images. The b_4 coefficient, position angle and ellipticity are different in B and K', which may be due to dust absorption in B. Our V and R band images suffer from poor S/N.

UGC 3536 : This galaxy has a significant dusty disk and the b_4 coefficient is disky. The disk is also evident in the $B-V$ and $B-R$ color maps. There is a constant rise in ellipticity for semi-major axis length < 19.5 arcsec, beyond which there is a decrease, which could be because of the disk.

UGC 3642 : The images for this galaxy show some kind of spiral structure, but this is not evident in the extinction or color maps. The b_4 coefficient is positive in the outer regions.

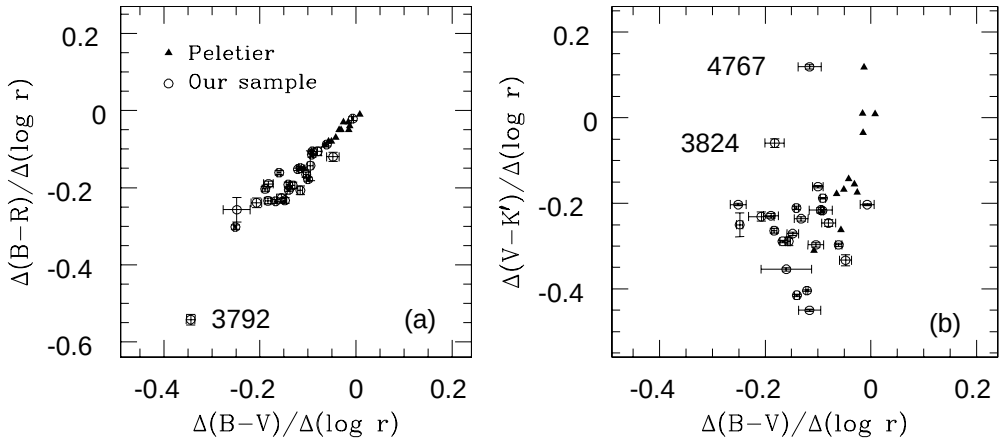

FIG. 5.— Correlation between different color gradients. The gradients for our sample and the sample of elliptical galaxies of Peletier et al. (1990a & b) are indicated with different symbols as in panel (a).

UGC 3792 : This galaxy is classified as S0 in the UGC but as SA0/a in the RC3 catalogue, and has no previous reported photometric study. The galaxy has a prominent dust lane along the major axis which greatly affects the various profiles. This dust lane is most prominent in the B band. The b_4 coefficient is positive in the outer region. There is a large color gradient in $B-V, B-R$ and $V-K'$, presumably because of the dust. A detailed study of this galaxy in the B, V, R, J, H, K' bands will be presented in a forthcoming paper.
UGC 4347 : Our $B-V$ and $B-K'$ color and extinction maps of this galaxy reveal a large dust patch near the center. The b_4 profile is disky throughout the observed region. Forbes & Thomson (1992) have detected possible shells in this galaxy. The extinction images in all bands shows faint structures, which may be responsible for the non-zero values the of b_4 coefficient.
UGC 4767 : The position angle and ellipticity profile for this galaxy are different in the B, R and K' bands for semi-major axis lengths < 5 arcsec, which could be because of a dust patch near the center of the galaxy. The various color maps also indicate the presence of the dust patch.
UGC 4901 : Our B band image of this galaxy has poor S/N. The color maps in $V-R$ and $V-K'$ show no features in the galaxy. The b_4 coefficient is positive towards the outer region, suggesting the presence of a faint disk.
UGC 7473 : This well studied edge-on lenticular galaxy forms a pair with NGC 4340. The surface brightness profile of this galaxy clearly indicates the presence of bulge and disk components. The Mg_2 line strength profiles along the major and minor axis of the galaxy differ dramatically and convincingly indicate the presence bulge and disk components (Fisher, Franx & Illingworth 1996). Michard & Marchal (1993) described UGC 7473 as having a disk fully embedded in a spheroidal halo. A disk of rapidly rotating gas is present within the inner 3 arcsec; this is decoupled from the stellar component (Fisher 1997). A concentration of dust in the disk has been proposed by Michard & Poulain (2000). Our $B-R$ and $B-K'$ color and extinction maps also reveal a clear inclined disk. The ellipticity rises from 0.2 to 0.61 over the observed region and the b_4 coefficient becomes significantly positive beyond 6 arcsec, which reflects the presence of a strong disk.
UGC 7880 : This galaxy forms a pair with NGC 4635, with a separation of at 1.5 arcmin. The ellipticity changes from 0.1 to 0.5 upto 10 arcsec, and decreases beyond that. The b_4 coefficient is positive upto the point at which the ellipticity begins to decrease. This may be due to the presence of an inner disk, the presence of which is also indicated by the $B-R$ and $B-K'$ color and extinction maps.
UGC 7933 : This galaxy is classified as S0 in the UGC, but as E1-2 in the RC3 catalogue. It forms a non-interacting pair with NGC 4670 at 5.6 arcmin separation. The B band image has poor S/N. The b_4 coefficient is positive towards the outer region. The color and extinction maps do not indicate any structure.
UGC 8675 : This is a little studied S0 galaxy hosting a Seyfert 1.5 nucleus, and has been classified as a SA0 galaxy in the RC3 catalogue. The isophotes of the galaxy are nearly circular and at 5 arcsec the ellipticity becomes 0.15 which is consistent with the values obtained by De Robertis, Hayhoe & Yee (1998) and Pierre et al. (2000). A dust absorption pattern is seen near the nucleus in the $B-R$ and $B-K'$ color and extinction maps. Pierre et al. (2000) have found from HST observations a U-shaped dust lane circling around the nucleus.

UGC 11178 : This galaxy has no previous reported photometric study. The extinction map show a ring like structure in all the bands. The ellipticity abruptly changes between 5 and 7 arcsec, which could be because of the ring like structure. The b_4 coefficient is significantly positive upto 7 arcsec. The color maps are featureless.
UGC 11356 : This is a face-on lenticular galaxy. A faint structure is apparent in extinction images in the optical bands near the center of the galaxy, but no features are obvious in the color maps.
UGC 11781 : This galaxy is classified as S0 in the UGC but as SAB in the RC3 catalogue. The presence of a bar is clear in the direct as well as extinction images. There is a dip in ellipticity profile at 10 arcsec, where there is a change in the position angle profile as well. The b_4 coefficient is positive in this region.
UGC 12655 : The $B-R$ and $B-K'$ color and extinction maps of this galaxy show a patchy region near the center of this galaxy. The b_4 coefficient is positive upto 8 arcsec.

REFERENCES

Abadi, M.G., Moore, B., & Bower, R.G. 1999, MNRAS, 308, 947
Bekki, K. 1998, ApJ, 504, 50
Bessell, M.S. 1990, PASP, 102, 1181
Bothun, G.D., & Gregg, M.D. 1990, ApJ, 350, 73
Chevalier, C., & Ilovaisky, S.A. 1991, A&AS, 90, 225
Cruz-Gonzalez, I., Carrasco, L., Ruiz, E., Salas, L., et al. 1994, RMxAA, 29, 197
De Robertis, M.M., Hayhoe, K., & Yee, H.K.C. 1998, ApJS, 115, 163
Fisher, D., Franx, M., & Illingworth, G. 1996, ApJ, 459, 110
Fisher, D. 1997, AJ, 113, 950
Forbes, D.A., & Thomson, R.C. 1992, MNRAS, 254, 723
Franx, M., Illingworth, G., & Heckman, T. 1989, AJ 98, 538
Frei, Z., & Gunn, J.E. 1994, AJ, 108, 1476
Fukugita, M., Shimasaku, K., & Ichikawa, T. 1995, PASP, 107, 945
Goudfrooij, P., Hansen, L., Jorgensen, H. E., et al. 1994, A&AS, 104, 179
Hubble, E.P. 1936, The Realm of the Nebulae, Yale Univ. Press, New Haven, reprinted by Dover Publ. Inc. New York (1958)
Hunt, L.K., Mannucci, F., Testi, L. et al. 1998, AJ, 115, 2594
Idiart, T.P., Michard, R., & de Freitas Pacheco, J.A. 2002, A&A, 383, 30
Jedrzejewski, R. I. 1987, MNRAS, 226, 747
Jorgensen, I., Franx, M., & Kjaergaard, P. 1992, A&AS, 95, 489
Jorgensen, I., Franx, M., & Kjaergaard, P. 1996, MNRAS, 280,167
Khosroshahi, H.G., Wadadekar, Y., & Kembhavi, A.K. 2000a, ApJ, 533, 162
Khosroshahi, H.G., Wadadekar, Y., Kembhavi, A.K., & Mobasher, B. 2000b, ApJ, 531, L103
Knapp, G.R., Guhathakurta, P., Kim, Dong-Woo, & Jura, M.A. 1989, ApJS, 70, 329
Landolt, A.U. 1992, AJ, 104, 340
Michard, R., & Marchal, J. 1993, A&AS, 98, 29
Michard, R. 2000, A&A, 369, 85
Michard, R., & Poulain, P. 2000, A&AS, 141, 1
Peletier, R.F., Davies, R.L., & Illingworth, G.D. 1990a, AJ, 100, 1091
Peletier, R.F., Valentijn, E.A., & Jameson, R.F. 1990b, A&A, 233, 62
Peletier, R.F., & Balcells, M. 1996, AJ, 111, 2238
Peletier, R.F., & Balcells, M. 1997, NewA, 1, 349
Persson, S.E., Frogel, J.A., & Aaronson, M. 1979, ApJS 39, 61
Pierre, F., Andrew, S.W., & Mulchaey, J. 2000, ApJS,128, 139
Pogge, R.W., & Eskridge, P.B. 1993, AJ, 106, 1405
Rieke, G.H. & Lebofsky, M.J. 1985, ApJ, 288, 618
Schlegel, D.J., Finkbeiner, D.P. & Davis, M. 1998, ApJ, 500, 525
Tadhunter, C.N., Morganti, R., di Serego-Alighieri, S., Fosbury, R.A.E., & Danziger, I.J. 1993, MNRAS, 263, 999
van den Bergh, S. 1994, AJ, 107, 153
Wadadekar, Y., Robbason, B. & Kembhavi, A.K. 1999, AJ, 117, 1219